Inorganic Chemistry

Article

pubs.acs.org/IC

# Heptacoordinated Molybdenum(VI) Complexes of Phenylenediamine Bis(phenolate): A Stable Molybdenum Amidophenoxide Radical

Mikko M. Hänninen,[†] Petriina Paturi,[‡] Heikki M. Tuononen,[†] Reijo Sillanpää,[†] and Ari Lehtonen*[,§]

[†]Department of Chemistry, P.O. Box 35, University of Jyväskylä, FI-40014 Jyväskylä, Finland

[‡]Wihuri Physical Laboratory, Department of Physics and Astronomy, University of Turku, FI-20014 Turku, Finland

[§]Department of Chemistry, University of Turku, FI-20014 Turku, Finland

Supporting Information

**ABSTRACT:** The syntheses, crystallographic structures, magnetic properties, and theoretical studies of two heptacoordinated molybdenum complexes with *N*,*N*′-bis(3,5-di-*tert*-butyl-2-hydroxyphenyl)-1,2-phenylenediamine ($H_4N_2O_2$) are reported. A formally molybdenum(VI) complex $[Mo(N_2O_2)Cl_2(dmf)]$ (**1**) was synthesized by the reaction between $[MoO_2Cl_2(dmf)_2]$ and $H_4N_2O_2$, whereas the other molybdenum(VI) complex $[Mo(N_2O_2)(HN_2O_2)]$ (**2**) was formed when $[MoO_2(acac)_2]$ was used as a molybdenum source. Both complexes represent a rare case of the $Mo^{VI}$ ion without any multiply bonded terminal ligands. In addition, molecular structures, magnetic measurements, ESR spectroscopy, and density functional theory calculations indicate that complex **2** is the first stable molybdenum(VI) amidophenoxide radical.

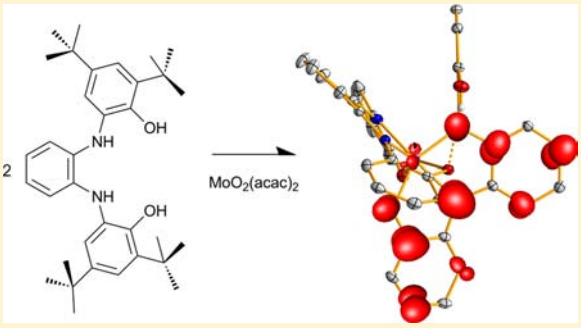


## INTRODUCTION

Redox-active catechols and *o*-aminophenols are of great interest as noninnocent ligands for their ability to contribute to the electronic properties typically associated with metal valence electrons.[1] One example of such ligands is *N*,*N*′-bis(3,5-di-*tert*-butyl-2-hydroxyphenyl)-1,2-phenylenediamine ($H_4N_2O_2$), which can be viewed as a dimeric derivative of two bidentate *o*-aminophenols.[2] Thus, it can act, once partially or fully deprotonated, as a multidentate ligand to form complexes with copper and zinc[2] as well as with titanium and zirconium.[3,4] This potentially tetradentate ligand has rich electrochemical behavior, and it can present five different oxidation states that are interrelated by one-electron-transfer steps (see Chart 1).

Oxomolybdenum(VI) complexes of various multidentate nitrogen-based ligands are known to behave as active catalysts in bioinspired oxotransfer reactions.[5−7] In the current contribution, we wanted to combine the redox-active nature of the ligand $H_4N_2O_2$ with the reactive $MoO_2$ functionality to generate new potential oxotransfer catalysts. However, in our experiments, the reaction of $H_4N_2O_2$ with several $MoO_2^{2+}$ sources did not yield the desired oxomolybdenum(VI) complex because the terminal oxo groups of the molybdenyl ion were removed upon ligand coordination. In the present paper, we report the syntheses, molecular structures, and magnetic behavior of two new molybdenum complexes with the $N_2O_2$ ligand. The synthesized heptacoordinated complexes $[Mo(N_2O_2)Cl_2(dmf)]$ (**1**) and $[Mo(N_2O_2)(HN_2O_2)]$ (**2**) are of interest because of their general coordination chemistry and the noninnocent behavior of the ligand. In support of the experimental work, we also carried out a comprehensive computational study to address the electronic nature of compounds **1** and **2**.

## RESULTS AND DISCUSSION

**Synthesis of 1.** The stoichiometric reaction of $[MoO_2Cl_2(dmf)_2]$ with $H_4N_2O_2$ in methanol or acetonitrile led to the rapid formation of an intensely colored solution, which afforded dark-green shiny air-stable crystals in high yield (Scheme 1). The crystals are practically insoluble in common organic solvents or water, which prevents any NMR analyses. The IR spectrum of the compound lacks the bands characteristic of a Mo=O function, which indicates the loss of molybdenyloxo groups during complexation. Structural analysis by X-ray crystallography (see below) shows that the solid-state structure of compound **1** consists of separate neutral molecules of $[Mo(N_2O_2)Cl_2(dmf)]$. Thus, in the formation of complex **1**, two metal−oxo bonds were cleaved while two metal−chloride bonds remained intact. This result was quite unexpected although similar reactivity with $MoO_2Cl_2$ derivatives was observed earlier.[8,9] In general, the cleavage of both metal−oxo bonds and the formation of a molybdenum(VI) compound without any multiply bonded terminal ligands are rare.[10] A structurally comparable 2,2′-biphenyl-bridged bis(2-aminophenol) ligand, 4,4′-di-*tert*-butyl-*N*,*N*′-bis(3,5-di-*tert*-butyl-2-hydroxyphenyl)-2,2′-diaminobiphenyl ($H_4{}^tBuClip$), was reported to react with $MoO_2(acac)_2$ to form $[MoO_2(H_2{}^tBuClip)]$, where the diarylamines remained proto-

**Received:** October 29, 2012
**Published:** April 29, 2013

   dx.doi.org/10.1021/ic302355b | *Inorg. Chem.* 2013, 52, 5714−5721

**Chart 1. Different Oxidation States of the Deprotonated Ligand $N_2O_2$ (Adapted from Reference 2)**

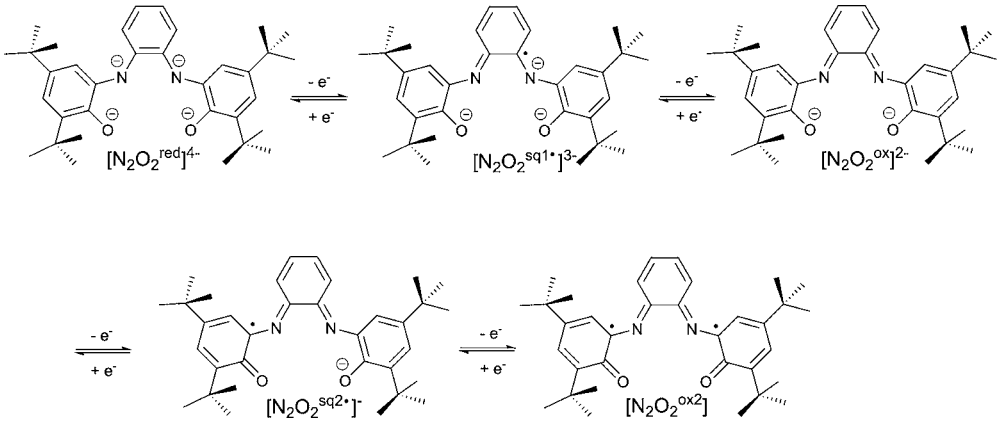


**Scheme 1. Formation of 1**

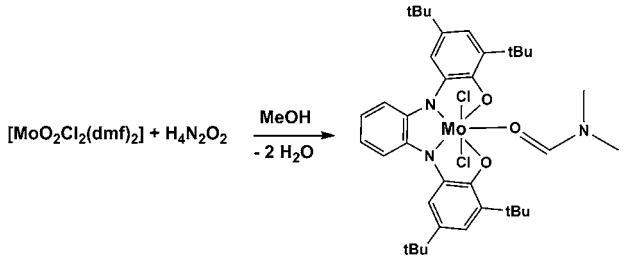


nated and bound trans to the terminal oxo groups.[10] In our studies, the elimination of both oxo moieties is probably due to the rigid geometry of the ligand system, which precludes formation of the favorable *cis*-$MoO_2$ structure. This and the relatively vague geometrical parameters of the product inspired us to study the bonding in detail (see below).

**Synthesis of 2.** When $[MoO_2(acac)_2]$ was reacted with $H_4N_2O_2$ in methanol, a dark solution was formed, upon which black shiny air-stable crystals of **2** deposited at ambient temperature (Scheme 2). The compound is soluble in

**Scheme 2. Formation of 2**[a]

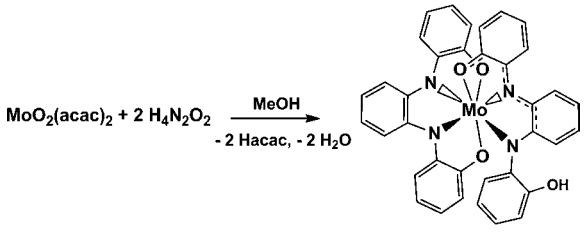


[a]The *tert*-butyl groups of the ligand $N_2O_2$ are omitted for clarity.

hydrocarbon solvents and ethers but virtually insoluble in methanol. The reaction was repeated in different stoichiometries to have identical product in lower yields without any sign of a 1:1 complex. Similar crystals were obtained using the structurally analogous $[MoO_2(Heg)_2]$ ($Heg^-$ = ethanediolate monoanion) as a starting material. The $^1H$ NMR spectrum of **2** does not offer any structural information because it shows only broad overlapping signals for the *tert*-butyl groups as well as for the hydrogen atoms in the aromatic rings. Similarly to **1**, the IR spectrum of **2** does not display any characteristic absorption for the Mo═O moiety. The structure of the compound was verified by X-ray crystallography (see below) to be a neutral molybdenum complex, where two different ligands are coordinated to the metal. The protonation states of the ligands were verified by the observation of a peak in the electrospray ionization mass spectrometry (ESI-MS) spectrum at the mass expected for the empirical formula. Interestingly, both ESI(+) and ESI(−) modes gave similar peak patterns with the characteristic isotope distribution of the metal. It seems that the molecular cation is formed as a result of removal of the odd electron, whereas the molecular anion is formed by reduction of the metal or pairing of the odd electron.

Analytical samples of **2** were obtained from freshly prepared reaction mixtures because the material seems to metamorphose upon standing for a longer period of time. Although the physical appearance and unit cell parameters of the crystals remain unchanged over time, their diffraction intensities decrease significantly. This causes refinement of the structure to fail because of the strong disorder of the ring atoms, which, in turn, suggests that the oxidation state of the ligand and/or metal can vary without any substantial changes in the overall molecular structure.

The cyclic voltammogram of **2** was measured in acetonitrile in the potential range from +2.0 to −1.7 V vs $Fc^+/Fc$. Three distinct one-electron oxidation waves (+0.41, +0.83, and +1.23 V) and three one-electron reduction waves (−0.01, −0.63, and −1.26 V) are seen within the solvent window (see the Supporting Information). For comparison, the ligand-based redox potentials for $[Zn(N_2O_2^{ox})]$ are seen at +0.03 and +0.37 V for oxidation and at −0.64 and −1.29 V for reduction.

## ■ STRUCTURAL STUDIES

Crystals of **1** were obtained from the reaction mixture in acetonitrile. In the solid-state structure (Figure 1), the molybdenum atom shares a plane with two oxygen atoms and two nitrogen atoms from the $N_2O_2$ ligand as well as with one oxygen donor from the coordinated dmf ligand. Two chlorides in axial positions complete the heptacoordinated environment around the metal center, which is best described as a distorted pentagonal bipyramid.[11] In principle, the protonation and oxidation level of the $H_4N_2O_2$ ligand can be determined from high-quality single-crystal X-ray data because the C−C, C−N, and C−O distances change systematically upon stepwise one-electron oxidation processes.[1] In **1**, the C−C bond lengths within both the phenolic parts of the $N_2O_2$ ligand and the central ring fall in the range 1.38−1.41 Å (Table 1), which does not allow unambiguous definition of the oxidation state of the ligand. Similarly, the C−N and C−O


dx.doi.org/10.1021/ic302355b | Inorg. Chem. 2013, 52, 5714−5721

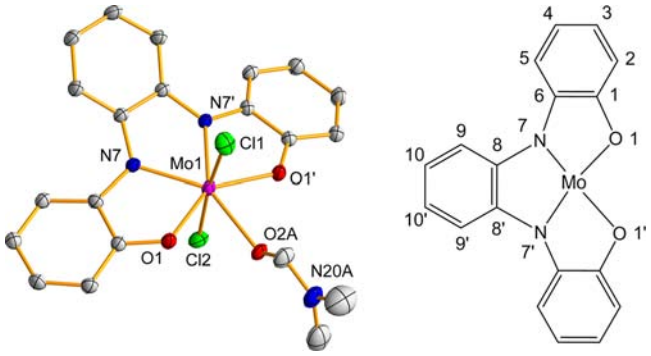


**Figure 1.** Crystal structure of **1** (left) and its numbering scheme (right). Symmetry operation: $x$, 0.5 − $y$, $z$. The C−H hydrogen atoms, *tert*-butyl substituents, and other parts of the disordered dmf molecule are omitted for clarity. Thermal ellipsoids are drawn at the 30% probability level.

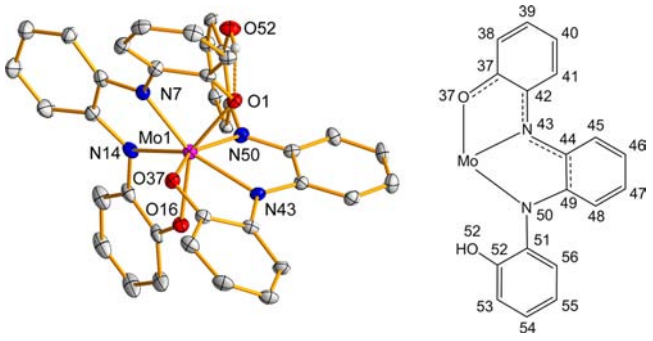


**Figure 2.** Crystal structure of **2** (left) and its numbering scheme (right). The C−H hydrogen atoms and *tert*-butyl substituents are omitted for clarity. Thermal ellipsoids are drawn at the 30% probability level.

bond distances of 1.398 and 1.322 Å, respectively, indicate that the ligand oxidation state might be either 1− or 2− (Chart 1), while the observed metal-to-donor atom distances are characteristic for anionic phenoxide and amide ligands. Consequently, theoretical calculations at the density functional theory (DFT) level were performed for a model system of **1** (see below).

The single crystals of **2** were separated from the methanol solution of the ligand and $[MoO_2(acac)_2]$ as described above. The X-ray structure (Figure 2) showed that the asymmetric unit consists of two crystallographically independent molecules with comparable structural parameters (Table 1). In these molecules, both the oxo moieties and the acetylacetonato ligands have been replaced during complexation, with the final product being a neutral heptacoordinated complex **2**, where the ligand displays two different coordination modes. One of the two ligands is fully deprotonated, whereas the other ligand has a dangling phenol part with an intact OH group. The formal oxidation state of the molybdenum center can again be estimated from the oxidation levels of these two different ligands. Similarly to complex **1**, the ligand assembly is not unambiguous because the quality of the X-ray data does now allow an in-depth analysis of the geometrical parameters. Nevertheless, the tetradentate ligand seems to be analogous to

**Table 1. Selected Geometrical Parameters of 1′ and 2′ Compared with the X-ray Data (For the Numbering Scheme, see Figures 1 and 2)**

| | | 1 | 1′-S | 1′-DR | | | 2a | 2b | $2^{AVG}$ | 2′-D |
|---|---|---|---|---|---|---|---|---|---|---|
| Mo | N7 | 2.065(2) | 2.034 | 2.077 | Mo1 | N43 | 2.149(3) | 2.152(4) | 2.151 | 2.167 |
| Mo | N7′ | 2.065(2) | 2.042 | 2.082 | Mo1 | N50 | 2.022(3) | 2.024(3) | 2.023 | 2.026 |
| Mo | O1 | 1.982(1) | 1.997 | 1.998 | Mo1 | O37 | 2.004(3) | 1.997(3) | 2.001 | 1.989 |
| Mo | O1′ | 1.982(1) | 1.966 | 1.970 | Mo1 | O52 | 3.566(4) | 3.574(4) | 3.570 | 3.632 |
| O1 | C1 | 1.322(2) | 1.312 | 1.309 | O37 | C37 | 1.324(6) | 1.344(6) | 1.334 | 1.313 |
| N7 | C6 | 1.398(3) | 1.390 | 1.378 | N43 | C42 | 1.375(5) | 1.377(6) | 1.376 | 1.357 |
| C1 | C2 | 1.407(3) | 1.398 | 1.400 | C37 | C38 | 1.412(6) | 1.404(6) | 1.408 | 1.403 |
| C2 | C3 | 1.380(3) | 1.384 | 1.382 | C38 | C39 | 1.375(7) | 1.385(7) | 1.380 | 1.380 |
| C3 | C4 | 1.411(3) | 1.400 | 1.404 | C39 | C40 | 1.415(7) | 1.402(6) | 1.409 | 1.407 |
| C4 | C5 | 1.376(3) | 1.385 | 1.382 | C40 | C41 | 1.397(6) | 1.388(7) | 1.393 | 1.378 |
| C5 | C6 | 1.401(3) | 1.396 | 1.399 | C41 | C42 | 1.391(7) | 1.401(7) | 1.396 | 1.406 |
| C6 | C1 | 1.400(3) | 1.392 | 1.398 | C37 | C42 | 1.426(6) | 1.427(5) | 1.427 | 1.421 |
| O1′ | C1′ | 1.322(2) | 1.309 | 1.307 | O52 | C52 | 1.375(6) | 1.374(5) | 1.375 | 1.345 |
| N7′ | C6′ | 1.398(3) | 1.387 | 1.376 | N50 | C51 | 1.431(5) | 1.445(6) | 1.438 | 1.424 |
| C1′ | C2′ | 1.407(3) | 1.399 | 1.401 | C52 | C53 | 1.403(6) | 1.414(7) | 1.409 | 1.401 |
| C2′ | C3′ | 1.380(3) | 1.383 | 1.381 | C53 | C54 | 1.395(7) | 1.382(6) | 1.389 | 1.384 |
| C3′ | C4′ | 1.411(3) | 1.402 | 1.405 | C54 | C55 | 1.400(9) | 1.390(8) | 1.395 | 1.394 |
| C4′ | C5′ | 1.376(3) | 1.385 | 1.382 | C55 | C56 | 1.378(6) | 1.386(7) | 1.382 | 1.385 |
| C5′ | C6′ | 1.401(3) | 1.398 | 1.401 | C56 | C51 | 1.397(7) | 1.390(6) | 1.394 | 1.393 |
| C6′ | C1′ | 1.400(3) | 1.390 | 1.398 | C51 | C52 | 1.390(8) | 1.376(8) | 1.383 | 1.397 |
| N7 | C8 | 1.388(2) | 1.375 | 1.369 | N43 | C44 | 1.359(5) | 1.367(5) | 1.363 | 1.350 |
| N7′ | C8′ | 1.388(2) | 1.375 | 1.369 | N50 | C49 | 1.383(5) | 1.383(6) | 1.383 | 1.372 |
| C8 | C9 | 1.405(3) | 1.396 | 1.398 | C44 | C49 | 1.422(6) | 1.442(7) | 1.432 | 1.428 |
| C9 | C10 | 1.378(3) | 1.392 | 1.394 | C44 | C45 | 1.412(6) | 1.397(6) | 1.405 | 1.407 |
| C10 | C10′ | 1.391(3) | 1.396 | 1.398 | C45 | C46 | 1.374(5) | 1.372(6) | 1.373 | 1.375 |
| C10′ | C9′ | 1.378(3) | 1.381 | 1.379 | C46 | C47 | 1.389(6) | 1.397(7) | 1.393 | 1.398 |
| C9′ | C8′ | 1.405(3) | 1.381 | 1.379 | C47 | C48 | 1.378(6) | 1.374(6) | 1.376 | 1.378 |
| C8′ | C8 | 1.401(3) | 1.400 | 1.407 | C48 | C49 | 1.406(5) | 1.389(5) | 1.398 | 1.400 |


dx.doi.org/10.1021/ic302355b | *Inorg. Chem.* 2013, 52, 5714−5721

a fully deprotonated $[N_2O_2^{red}]^{4-}$ (Chart 1) as in **1**, whereas the tridentate ligand with a dangling phenol part can be best described as a triply deprotonated ligand $[HN_2O_2^{sq1\bullet}]^{2-}$ (Chart 1). With these presumptions, the formal oxidation state of the metal center is molybdenum(VI). Because the oxidation level assumed for the tridentate ligand involves one unpaired electron, the material should be paramagnetic.

## MAGNETIC PROPERTIES

Compound **1** showed only a diamagnetic signal, as expected because of the even number of electrons. Compound **2**, on the other hand, gave a paramagnetic signal with susceptibility $\chi_{mol}$ = 4.2 × $10^{-7}$ $m^3$/mol at 5 K ($\chi_{mol} = M\chi_v/\rho$, where $\rho$ is the density, $M$ is the molar mass, and $\chi_v$ is the volume magnetic susceptibility). The temperature dependence of the susceptibility was also measured, and the data were fitted to the Curie law of localized moments, $\chi_{mol} = C/(T - \theta_p)$. Figure 3 shows

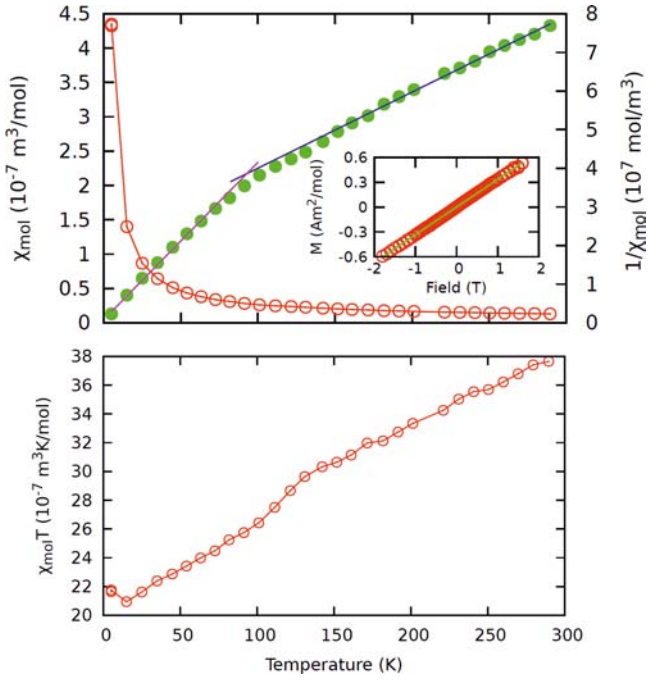


**Figure 3.** Plot of the susceptibility $\chi_{mol}$ versus $T$ (top) and $\chi_{mol}T$ versus $T$ (bottom) of compound **2** in a 0.1 T field. The green dotted values show $1/\chi_{mol}$ with a fit to the Curie law at the high- (blue line) and low-temperature (violet line) regime. The inset shows the magnetic field dependence at 5 K, with a linear fit giving $\chi_{mol}$ = 4.2 × $10^{-7}$ $m^3$/mol.

the $\chi_{mol}T$ versus $T$ plot of **2** (bottom) as well as the plots of $\chi_{mol}$ versus $T$ and $1/\chi_{mol}$ versus $T$ (top). As can be seen from the figure, the inverse of the susceptibility does not obey the Curie law, which means that the magnetic spin is not localized. However, $\chi_{mol}$ is not temperature-independent either, as would be expected for Pauli paramagnetism induced by a completely nonlocalized electron. Consequently, the most probable explanation of the data measured for compound **2** is a partially localized unpaired electron, which causes the magnetic properties.[12] The calculated magnetic moment ($\mu_{eff}$) at the high-temperature range ($T$ > 150 K) is 1.80 $\mu_B$, whereas it is 1.25 $\mu_B$ at the low-temperature range ($T$ < 80 K). Because the "spin-only" value for an unpaired electron is 1.73 $\mu_B$, the magnetic moment at the high-temperature range clearly indicates the presence of only one unpaired electron.

## ELECTRON-SPIN RESONANCE (ESR) SPECTROSCOPY

X-band ESR spectra of the solid compounds **1** and **2** were measured at room temperature as well as at 4 K, whereas the solution spectrum of **2** was measured in $CH_2Cl_2$ at room temperature. As expected, compound **1** did not show an ESR signal, while a solid sample of **2** gave an axial spectrum at 4 K with $g_\perp$ = 2.0157 and $g_\parallel$ = 2.0047 (see the Supporting Information). Thus, the calculated $\Delta g$ = 0.011 and $\langle g \rangle$ = 2.012. In $CH_2Cl_2$, **2** produced a nearly isotropic ESR signal ($S = {}^1/_2$) $g_{iso}$ = 2.0087 with minor asymmetry, possibly because of an unresolved hyperfine interaction. These values clearly indicate that the unpaired electron is predominantly on the orbitals of the ligand, in a fashion similar to that in nickel(II) and ruthenium(II) semiquinone complexes,[13] and not on the metal because $\langle g \rangle$ varies from 1.938 to 1.952 in several octahedral molybdenum(V) compounds.[14] Against this scenario, **2** is best described as a molybdenum(VI) complex with a semiquinone-type radical ligand.

## THEORETICAL STUDIES

Because the oxidation state of the ligands in **1** and **2** cannot be explicitly determined from the X-ray diffraction data, DFT calculations were performed to shed light on the electronic structure and bonding of the ligands in these complexes. Generally, in the noninnocent $C_6H_4(NR)_2$-*o* and $C_6H_4(O)$-(NR)-*o* species (R = H, alkyl, aryl), discrimination between the completely reduced amido and phenoxido or oxidized imino and quinone formulation of the ligand is done by inspecting the trends in the experimentally determined C−C, C−N, and C−O bond distances, which obviously requires very high-quality X-ray diffraction data.[1,15,16] In addition, the partially reduced radical *o*-benzosemiquinoneiminato form should be recognizable by comparison of these bond distances.[17] As earlier studies have shown,[18] computational analyses provide in many cases crucial information in the determination of the electronic nature of the coordinating ligand and that of the entire complex, especially when the experimental structural data are inconclusive.

In order to determine the correct electronic states of the metals and ligands in both **1** and **2**, the geometries of model complexes **1′** and **2′** (*tert*-butyl substituents replaced with methyl groups) were optimized using the PBE1PBE[19] functional and def2-TZVP[20] basis sets. The nature of the stationary points found was addressed by the subsequent calculation of two of the lowest eigenvalues of the Hessian matrix. Selected geometrical parameters of the optimized structures are given in Table 1.

For **1**, there exist three plausible electronic states: a closed-shell singlet **1′**-S, a high-spin triplet **1′**-T, and a broken-symmetry singlet diradical **1′**-DR. Geometry optimizations were performed for all of these states, and the results indicate that the triplet state is about 30 kJ/mol higher in energy than either of the two singlet states (in agreement with magnetometric measurements) and therefore will not be discussed further. From the two singlet states, the ground state is the diradical state **1′**-DR, which, however, is only 5 kJ/mol lower in energy than **1′**-S. Considering such a small energy difference between these states, the diradical nature of complex **1** is relatively small, which is also evident from the calculated frontier molecular orbitals (MOs; see below) and from the spin distribution of the broken-symmetry solution (Figure 4).


dx.doi.org/10.1021/ic302355b | Inorg. Chem. 2013, 52, 5714−5721

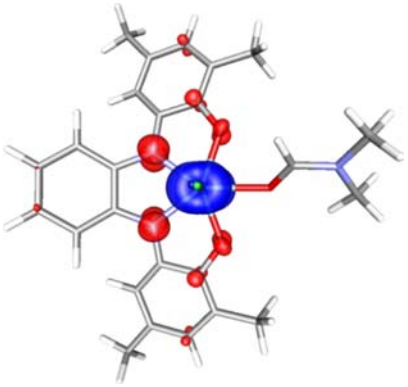

**Figure 4.** Calculated spin density distribution of complex **1′**-DR. Red and blue denote excess $\alpha$ and $\beta$ spin density, respectively.

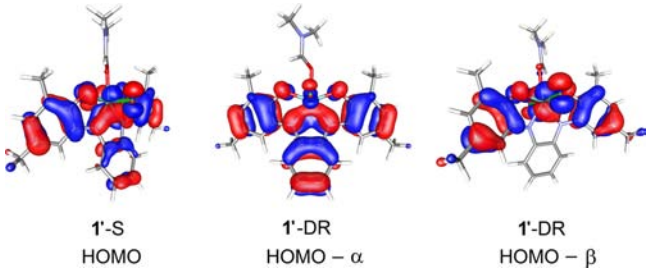


**Figure 5.** Frontier MOs of **1′**-S and **1′**-DR. The Mulliken populations of the orbitals shown are presented in the Supporting Information.

According to the Mulliken population analysis and the calculated spin density,[21] the formally unpaired electrons in **1′**-DR are localized mostly at the nitrogen atoms of the ligand and at the molybdenum center. The diamagnetism in **1′**-DR is then due to the relatively strong antiferromagnetic coupling between these electrons, which results in an $S = 0$ state.

A detailed comparison between the X-ray data of **1** and the theoretical results for **1′**-S and **1′**-DR shows a good overall agreement, although some differences can also be observed. Most notably, the coordinated dmf molecule is tilted in both optimized structures, which breaks the molecular symmetry of the complex. This behavior is, however, entirely expected when considering the observed disorder in the experimental X-ray data. For both **1′**-S and **1′**-DR, the largest deviation between the calculated and experimental bond lengths is about 0.04 Å, and all important bond lengths in the complex (including those in *o*-phenylenediamine and *o*-aminophenol rings) are reproduced with good precision ($R_{par}$[22] values 0.0072 and 0.0045, respectively). The single biggest difference between the structures **1′**-S and **1′**-DR is in the Mo−N bond distances, which are about 0.04 Å longer in **1′**-DR and thereby in slightly better agreement with the experimental data. However, the differences in the optimized bond lengths of **1′**-S and **1′**-DR are, in general, too small in order for any definite conclusions to be drawn about the nature of the electronic ground state of **1**.

The concept of metrical oxidation state (MOS) was introduced recently by Brown,[23] and it has been used to quantify the formal oxidation state of noninnocent (oxidized) amidophenoxide or catecholate ligands coordinated to metal ions by examination of their geometrical parameters. The MOS calculated for the experimental structure **1** is 1.55(14). Corresponding values for the DFT-optimized structures **1′**-S and **1′**-DR are 1.58(17) and 1.47(15), respectively. From these, the data for **1′**-S are in slightly better agreement with the experimental value, although the estimated standard deviations are very high, preventing definite conclusions from being made. As explained by Brown, compounds with metal ions in the high oxidation state and with two or fewer d electrons, such as molybdenum(VI) and vanadium(V) complexes, tend to have noninteger MOS values that originate from ligand-to-metal $\pi$ donation rather than from an antiferromagnetic coupling of electrons residing in separate orbitals.[23] Considering complex **1**, a visual inspection of frontier MOs of **1′**-S and **1′**-DR shows significant delocalization, which in both cases gives rise to $\pi$ bonding between the *o*-phenylenediamine fragment of the ligand and the molybdenum ion (Figure 5). This not only explains the similarity in the calculated MOS values for **1′**-S and **1′**-DR but also supports the earlier conclusions of the rather small effect that the diradical character has on the overall electronic structure of **1′** (see above).

In summary, although the experimental structural data show some discrepancies between the expected and observed bond lengths, the results from theoretical calculations indicate that the ground state of **1** is a singlet with a small diradical character, which cannot therefore be fully described with a closed-shell configuration. The observed deviations in the geometrical parameters of the phenyl rings and Mo−N/O bonds can be attributed primarily to $\pi$ donation from the ligand to the high-valent molybdenum cation rather than actual electron transfer creating a lower-oxidation-state molybdenum(V) center.

In a fashion similar to that of **1**, the geometrical parameters of the tridentate ligand in complex **2** suggest some variation in the oxidation state of the ligand, which is also evident from the odd number of electrons in this complex. The plausible electronic states for **2** are a doublet (**2′**-D) and a quartet (**2′**-Q). Thus, DFT optimizations were performed to estimate the energy difference between the two states, and the results show the quartet state to be over 80 kJ/mol higher in energy compared to the doublet. It is important to note that a broken-symmetry doublet with two unpaired electrons at the ligand and one at the metal center (coupled antiferromagnetically as in **1′**-DR) is also a plausible electronic configuration. However, we were not able to locate a minimum corresponding to such a state; the Mulliken populations in the highest occupied molecular orbital (HOMO; singly occupied molecular orbital, SOMO−1) of **2′**-D also have insignificant (only a few percent) contributions from the metal orbitals, thus excluding the possibility of a broken-symmetry-type state (see the Supporting Information). Hence, the ground state of complex **2** was inferred to be a pure doublet, which is fully supported by the data from magnetometric measurements (see above).

The theoretical model **2′**-D reproduces the experimental geometrical features of **2** from good-to-excellent precision (the $R_{par}$ value for bond distances from Table 1 is 0.0056, excluding the distance between the uncoordinated O52 and Mo1). The calculated data reproduce the key bond lengths around the metal center and show that the Mo−N(radical) bond length is significantly longer (over 0.1 Å) compared with the Mo−N(amido) bond. The structural parameters also show the overall shortening of bonds around the N43 center compared to the amido nitrogen atom because the latter bonds are about 0.02−0.07 Å longer than the former. In addition, small changes in the C−C and C−O bond distances of the neighboring phenyl groups of N43 indicate delocalization of the unpaired electron density over the whole aromatic system. The delocalization is also visible in the calculated spin distribution


dx.doi.org/10.1021/ic302355b | Inorg. Chem. 2013, 52, 5714−5721

of **2′** (Figure 6), which, together with the Mulliken population analysis, shows the unpaired electron to be delocalized over the

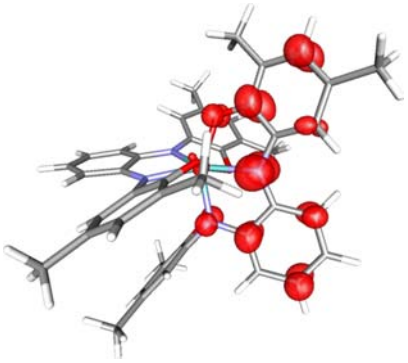

**Figure 6.** Calculated spin density distribution of complex **2**.

aromatic rings of the tridentate ligand, with roughly one-third of the total spin density attributable to the N43 atom.

MOSs were calculated for the experimental structure of **2** (two separate molecules in the asymmetric unit) and for the theoretical model **2′**-D. The MOS calculated for **2** from the average experimental bond distance is 1.50(7), whereas the MOSs calculated separately for the individual molecules in the asymmetric unit are 1.42(10) and 1.58(6). The corresponding MOS value for the DFT-optimized structure is 1.30(9), which differs slightly from the experimental data, although the differences are again within $2\sigma$. These results clearly point out the sensitivity of MOS analysis to the X-ray data, which prevents an in-depth discussion of the electronic structure of **2**. Similarly to **1**, the calculated noninteger MOSs can be attributed to $\pi$ donation from the ligand to the high-valent molybdenum cation [with the formal oxidation state of molybdenum(VI)] rather than to any actual ligand-to-metal electron transfer.

Considered as a whole, the conducted experimental and theoretical investigations present an unambiguous picture of the electronic state and bonding in **2**. To the best of our knowledge, this complex represents the first example of a stable high-valent molybdenum amidophenoxide radical.

## CONCLUSIONS

The redox-active and potentially tetradentate phenolic ligand precursor $H_4N_2O_2$ reacts with $[MoO_2Cl_2(dmf)_2]$ to form a heptacoordinated molybdenum(VI) complex **1**, where the tetradentate ligand is fully deprotonated. In contrast, the reaction of the precursor with $[MoO_2(acac)_2]$ leads to the formation of **2**. Both of the prepared complexes present the rare situation of a molybdenum(VI) ion without any multiply bonded terminal ligands. Furthermore, in complex **2**, the noninnocent ligands display both tetradentate and tridentate coordination modes, with the latter one containing an unpaired electron and thereby forming the first example of a stable molybdenum amidophenoxide radical.

## EXPERIMENTAL SECTION

**Methods and Materials.** The starting complexes $[MoO_2Cl_2(dmf)_2]$, $[MoO_2(acac)_2]$, and $[MoO_2(Heg)_2]$ were synthesized by literature procedures.[24−26] The ligand precursor was prepared and purified according to a published synthesis.[1,3b] Other chemicals were used as purchased from commercial sources. The solvents used were of high-performance liquid chromatography grade. All syntheses were done under an ambient atmosphere.

ESI-MS for **2** was measured in the positive- and negative-ion mode with a Bruker micrOTOF-Q spectrometer. The samples were injected as methyl cyanonitrile (MeCN)−water solutions. Cyclic voltammetry (CV) for **2** was recorded at ambient temperature using a platinum working electrode, a 1-mm-diameter platinum counter electrode, and a Ag/AgCl reference electrode. Samples were dissolved in MeCN containing 0.1 M $(Bu_4N)ClO_4$ as the supporting electrolyte. The voltammograms were recorded at a scan rate of 100 mV/s, while the potentials were measured in volts versus the $Fc^+/Fc$ couple.

Solid-state ESR spectra were recorded at 4 K using a 9 GHz X-band EPR spectrometer, whereas the solution ESR of **2** (in $CH_2Cl_2$) was recorded at ambient temperature. The magnetic properties were measured in a SQUID magnetometer with 70 and 48 mg samples of **1** and **2**, respectively, sealed in plastic nonmagnetic straws. The temperature dependence from 5 to 300 K was measured in a 0.1 T magnetic field using 10 K steps and the field dependence was measured at 5 K between −2 and 2 T using 50 mT steps. The susceptibility of sample **2** was determined at 5 K from a linear fit to the $M(B)$ data.

*Preparation of* **1**. To a solution of $[MoO_2Cl_2(dmf)_2]$ (173 mg, 0.50 mmol) in acetonitrile (5 mL) was added 260 mg (0.50 mmol) of the ligand precursor dissolved in 10 mL of the same solvent. The resulting intensely dark solution was stored for 2 days at room temperate to give dark crystals. Crystals were isolated by filtration and washed with 10 mL of acetonitrile to obtain dark-green prisms in 63% (250 mg) yield. Elem anal. Calcd for $C_{39}H_{54}Cl_2MoN_4O_3$: C, 59.01; H, 6.86; N, 7.06. Found: C, 59.25; 7.02; N, 6.80. IR: 1642 (vs), 1460 (vs), 1377 (s), 1366 (s), 1312 (w), 1289 (w), 1277 (w), 1250 (m), 1189 (w), 1167 (m), 1134 (w), 1111 (w), 1076 (w), 997 (w), 922 (w), 872 (w), 762 (w), 755 (m), 721 (w), 608 (w), 488 (w) $cm^{-1}$. Complete insolubility of the solid compound prevented further spectroscopic analyses.

*Preparation of* **2**. A solution of $H_4N_2O_2$ (172 mg, 0.33 mmol) in 10 mL of methanol was added to a solution of $[MoO_2(acac)_2]$ (55 mg, 0.17 mmol) in 10 mL of the same solvent. A dark-bluish color developed rapidly, and black shiny crystals were formed over 24 h at room temperature. The crystals were collected by filtration and washed with 10 mL of methanol to obtain **2** in 75% yield (280 mg). Elem anal. Calcd for $C_{68}H_{90}MoN_4O_4$: C, 72.70; H, 8.07; N, 4.99. Found: C, 73.42; H, 8.61; N, 5.04. IR: 1460 (vs), 1380 (s), 1362 (s), 1300 (s, br), 1285 (m), 1260 (m), 1236 (s), 1202 (w), 1130 (m), 1072 (w), 1018 (w), 993 (m), 883 (w), 872 (w), 770 (w), 740 (m), 731 (m), 605 (w), 606 (w) $cm^{-1}$. $^1H$ NMR ($CDCl_3$): $\delta$ 0.9−2.1 (72 H, several overlapping peaks), 6.8−7.1 (16 H, several broad peaks). ESI(+)-MS: $m/z$ 1123.5862 ($M^+$, calcd $m/z$ 1123.59382). ESI(-)-MS: $m/z$ 1123.5915 ($M^-$, calcd $m/z$ 1123.59382).

**X-ray Crystallographic Details.** Crystals suitable for single-crystal X-ray measurements were obtained directly from the reaction mixtures. The crystallographic data for compounds **1** and **2** are summarized in Table 2 along with other experimental details. The data sets were collected at 223 K (**1**) or at 173 K (**2**) with an Enraf Nonius Kappa CCD area-detector diffractometer with the use of graphite-monochromated Mo K$\alpha$ radiation ($\lambda$ = 0.71073 Å). Data collection was performed using $\varphi$ and $\omega$ scans, and the data were processed using *DENZO-SMN v0.93.0*.[27] *SADABS*[28] absorption correction was applied for complex **2**. The structures were solved by direct methods using *SHELXS-97*,[29] and full-matrix least-squares refinements on $F^2$ were performed using *SHELXL-97*.[27] All figures were drawn with *DIAMOND 3*.[30] For all compounds, the heavy atoms were refined anisotropically, whereas all hydrogen atoms were included at the calculated distances with fixed displacement parameters from their host atoms (1.2 or 1.5 times the host atom).

**Computational Details.** All calculations were performed using the *TURBOMOLE 6.3* program package.[31] The geometries of the complexes were optimized using the PBE1PBE[19] functional and Ahlrichs' def2-TZVP[20] basis sets. The nature of the stationary points found was assessed by calculating the two lowest eigenvalues of the Hessian matrix. Mulliken population analyses were performed as


dx.doi.org/10.1021/ic302355b | *Inorg. Chem.* 2013, 52, 5714−5721

**Table 2. Summary of Crystallographic Data for 1 and 2 at 223 and 173 K, Respectively**

| | 1 | 2 |
|---|---|---|
| formula | $C_{39}H_{54}C_{12}MoN_4O_3$ | $C_{68}H_{89}MoN_4O_4$ |
| $M_r$ | 793.70 | 825.74 |
| cryst syst | monoclinic | monoclinic |
| space group | $P2_1/m$ (No. 11) | $C2/c$ (No. 15) |
| $a$/Å | 9.8327(2) | 30.4051(3) |
| $b$/Å | 18.5416(3) | 18.9197(2) |
| $c$/Å | 11.3473(2) | 45.7404(5) |
| $\alpha$/deg | 90.00 | 90.00 |
| $\beta$/deg | 99.8100(10) | 104.2260(10) |
| $\delta$/deg | 90.00 | 90.00 |
| $V$/Å$^3$ | 2036.66(6) | 25505.5(5) |
| $Z$ | 2 | 16 |
| $\mu$(Mo K$\alpha$)/mm$^{-1}$ | 0.492 | 0.254 |
| no. of obsd reflns | 7964 | 15921 |
| $R_{int}$ | 0.0189 | 0.0226 |
| no. of param | 290 | 1393 |
| R1[a] | 0.0405 (0.0314) | 0.0808 (0.052) |
| wR2[a] | 0.0779 (0.0724) | 0.114 (0.102) |
| GOF | 1.057 | 1.053 |
| peak, hole/(e/Å$^3$) | 0.324, −0.435 | 0.468, −0.372 |

[a]The values in parentheses are for reflections with $I > 2.0\sigma(I)$. R1 = $\sum||F_o| - |F_c||/\sum|F_o|$. wR2 = $\{\sum[w(F_o^2 - F_c^2)^2]/\sum[w(F_o^2)^2]\}^{1/2}$, where $w = 1/[\sigma^2(F_o^2) + (aP)^2 + bP)]$ and $P = (2F_c^2 + F_o^2)/3$.

implemented in the *TURBOMOLE 6.3* code. The program *gOpenMol*[32] was used for visualizations of the spin density and MOs.

## ■ ASSOCIATED CONTENT

### Supporting Information

Experimental crystallographic information of **1** and **2** in CIF format, as well as optimized structures, data from Mulliken population analyses, and calculated spin densities of **1′** and **2′**. This material is available free of charge via the Internet at http://pubs.acs.org.

## ■ AUTHOR INFORMATION

### Corresponding Author

*E-mail: ari.lehtonen@utu.fi. Tel: +358-2-333-6733. Fax: +358-2-333-6700.

### Notes

The authors declare no competing financial interest.

## ■ ACKNOWLEDGMENTS

The authors thank Dr. Pasi Virta for mass spectra and Dr. Pia Damlin for CV measurements. H.M.T. and M.M.H. acknowledge financial support from the Technology Industries of the Finland Centennial Foundation. Part of this work was also supported by the COST Action CM1003: "Biological oxidation reactions—mechanisms and design of new catalysts".

## ■ REFERENCES

(1) (a) Kaim, W.; Schwederski, B. *Coord. Chem. Rev.* **2010**, *254*, 1580. (b) Kaim, W. *Inorg. Chem.* **2011**, *50*, 9752.
(2) Chauduri, P.; Hess, M.; Müller, J.; Hildenbrand, K.; Bill, E.; Weyhermüller, T.; Wieghardt, K. *J. Am. Chem. Soc.* **1999**, *121*, 9599.
(3) (a) Blackmore, K. J.; Lal, N.; Ziller, J. W.; Heyduk, A. F. *J. Am. Chem. Soc.* **2008**, *130*, 2728. (b) Blackmore, K. J.; Lal, N.; Ziller, J. W.; Heyduk, A. F. *Eur. J. Inorg. Chem.* **2009**, 735.
(4) Zelikoff, A. L.; Kopilov, J.; Goldberg, I.; Coates, G. W.; Kol, M. *Chem. Commun.* **2009**, 6804.
(5) Dinda, R.; Sengupta, P.; Ghosh, S.; Sheldrick, W. S. *Eur. J. Inorg. Chem.* **2003**, 363.
(6) Pramanik, N. R.; Ghosh, S.; Raychaudhuri, T. K.; Ray, S.; Butcher, R. J.; Mandal, S. S. *Polyhedron* **2004**, *23*, 1595.
(7) Mayilmurugan, R.; Harum, B. N.; Volpe, M.; Sax, A. F.; Palaniandavar, M.; Mösch-Zanetti, N. C. *Chem.—Eur. J.* **2011**, *17*, 704.
(8) (a) Hanna, T. A.; Incarvito, C. D.; Rheingold, A. L. *Inorg. Chem.* **2000**, *39*, 630. (b) Hanna, T. A.; Ghosh, A. K.; Ibarra, C.; Mendez-Rojas, M. A.; Rheingold, A. L.; Watson, W. H. *Inorg. Chem.* **2004**, *43*, 1511. (c) Hanna, T. A.; Ghosh, A. K.; Ibarra, C.; Zakharov, L.; Rheingold, A. L.; Watson, W. H. *Inorg. Chem.* **2004**, *43*, 7567. (d) Liu, L.; Zakharov, L. N.; Golen, J. A.; Rheingold, A. L.; Watson, W. H.; Hanna, T. A. *Inorg. Chem.* **2006**, *45*, 4247.
(9) Lehtonen, A.; Balcar, H.; Sedláček, J.; Sillanpää, R. *J. Organomet. Chem.* **2008**, *693*, 1171.
(10) Kopec, J. A.; Shekar, S.; Brown, S. N. *Inorg. Chem.* **2012**, *51*, 1239.
(11) Casanova, D.; Alemany, P.; Bofill, J. M.; Alvarez, S. *Chem.—Eur. J.* **2003**, *9*, 1281.
(12) Mohn, P. *Magnetism in the solid state—an introduction*; Springer-Verlag: Berlin, 2003.
(13) (a) Ottenwaelder, X.; Ruiz-García, R.; Blondin, G.; Carasco, R.; Cano, J.; Lexa, D.; Journaux, Y.; Aukauloo, A. *Chem. Commun.* **2004**, 504. (b) Waldhör, E.; Schwederski, B.; Kaim, W. *J. Chem. Soc., Perkin Trans. 2* **1993**, 2109.
(14) Xiao, Z.; Bruck, M. A.; Doyle, C.; Enemark, J. H.; Grittini, C.; Gable, R. W.; Wedd, A. G.; Young, C. G. *Inorg. Chem.* **1995**, *34*, 5950.
(15) Khusniyarov, M. M.; Harms, K.; Burghaus, O.; Sundermeyer, J.; Sarkar, B.; Kaim, W.; van Slageren, J.; Duboc, C.; Fiedler, J. *Dalton Trans.* **2008**, 1355.
(16) Chaudhuri, P.; Verani, C. N.; Bill, E.; Bothe, E.; Weyhermüller, T.; Wieghardt, K. *J. Am. Chem. Soc.* **2001**, *123*, 2213.
(17) Bhattacharya, S.; Gupta, P.; Basuli, F.; Pierpont, C. G. *Inorg. Chem.* **2002**, *41*, 5810.
(18) (a) Bachler, V.; Olbrich, G.; Neese, F.; Wieghardt, K. *Inorg. Chem.* **2002**, *41*, 4179. (b) Das, D.; Sarkar, B.; Mondal, T. K.; Mobin, S. M.; Fiedler, J.; Kaim, W.; Lahiri, G. M. *Inorg. Chem.* **2011**, *50*, 7090. (c) Lu, C. C.; DeBeer George, S.; Weyhermüller, T.; Bill, E.; Bothe, E.; Wieghardt, K. *Angew. Chem., Int. Ed.* **2008**, *47*, 6384. (d) Tomson, N. C.; Labios, L. A.; Weyhermüller, T.; Figueroa, J. S.; Wieghardt, K. *Inorg. Chem.* **2011**, *50*, 5763.
(19) (a) Perdew, J. P.; Burke, K.; Ernzerhof, M. *Phys. Rev. Lett.* **1996**, *77*, 3865. (b) Perdew, J. P.; Burke, K.; Ernzerhof, M. *Phys. Rev. Lett.* **1997**, *78*, 1396. (c) Perdew, J. P.; Ernzerhof, M.; Burke, K. *J. Chem. Phys.* **1996**, *105*, 9982. (d) Adamo, C.; Barone, V. *J. Chem. Phys.* **1999**, *110*, 6158.
(20) (a) Weigend, F.; Häser, M.; Patzelt, H.; Ahlrichs, R. *Chem. Phys. Lett.* **1998**, *294*, 143. (b) Weigend, F.; Ahlrichs, R. *Phys. Chem. Chem. Phys.* **2005**, *7*, 3297.
(21) Mulliken, R. S. *J. Chem. Phys.* **1955**, *23*, 1833.
(22) $R_{par}$ is defined as $R_{par} = (\sum|P_{exp} - P_{theo}|)/\sum|P_{exp}|$ and can be used to quantitatively measure the fit of theoretical model to the experimental one.
(23) Brown, S. N. *Inorg. Chem.* **2012**, *51*, 1251.
(24) Schröder, F. A.; Scherle, J. *Z. Naturforsch.* **1973**, *28b*, 46.
(25) Arnaiz, F. J.; Aguado, R.; Sanz-Aparicio, J.; Marinez-Ripoli, M. *Polyhedron* **1994**, *13*, 2745.
(26) Chen, G. J.-J.; McDonald, J. W.; Newton, W. E. *Inorg. Chem.* **1976**, *15*, 2612.
(27) Otwinowski, Z. W. In *Minor in Methods in Enzymology*; Carter, C. W., Sweet, R. M., Eds.; Academic Press: New York, 1997; Vol. *276*, Part A, pp 307−326.
(28) Sheldrick, G. M. *SADABS*; University of Göttingen: Göttingen, Germany, 2002.
(29) Sheldrick, G. M. *Acta Crystallogr.* **2008**, *A64*, 112.
(30) Brandenburg, K.; Putz, H. *DIAMOND—Crystal and Molecular Structure Visualization*; Crystal Impact: Bonn, Germany.
(31) *TURBOMOLE V6.3 2011*, a development of University of Karlsruhe and Forschungszentrum Karlsruhe GmbH, 1989−2007,

TURBOMOLE GmbH since 2007; available from http://www.turbomole.com.
(32) (a) Laaksonen, L. *J. Mol. Graphics* **1992**, *10*, 33. (b) Bergman, D. L.; Laaksonen, L.; Laaksonen, A. *J. Mol. Graphics* **1997**, *15*, 301.